Characterization and Evaluation of Supported *rac*-Dimethylsilylenebis(indenyl)zirconium Dichloride on Ethylene Polymerization

Fernando C. Franceschini,[1] Tatiana T. da R. Tavares,[1] Daniela Bianchini,[2] Maria do Carmo M. Alves,[2] Maria Lujan Ferreira,[3] João H. Z. dos Santos[2]

[1]*Ipiranga Petroquímica S. A., Divisão de Desenvolvimento e Especialidades, Departamento de Desenvolvimento de Produto, Pólo Petroquímico do Sul, Rodovia Tabaí Canoas, km 419, CEP 95853-000, Triunfo, Brazil*
[2]*Instituto de Química da Universidade Federal do Rio Grande do Sul, Av. Bento Gonçalves, 9500, CEP 91501-970, Porto Alegre, Brazil*
[3]*Planta Piloto de Ingeniería Quimica (PLAPIQ)–Universidad Nacional del Sur (UCS)–Consejo Nacional de Investigaciones Cientificas y Técnicas (CONICET), Camino La Carindanga Km 7, CC 717 8000 Bahia Blanca, Argentina*

Received 20 November 2007; accepted 12 October 2008
DOI 10.1002/app.29430
Published online 2 January 2009 in Wiley InterScience (www.interscience.wiley.com).

ABSTRACT: *rac*-Dimethylsilylenebis(indenyl)zirconium dichloride was grafted onto commercial methyl aluminoxane modified silica (SMAO) at different loadings (0.1–1.5 wt % Zr/SMAO). Supported catalysts were evaluated in ethylene polymerization with isoprenylaluminum as a cocatalyst. The characterization of two supported catalysts bearing 0.3 and 0.8 wt % Zr/SiO_2 by extended X-ray absorption fine structure indicated that the number and the intensity of the peaks beyond the coordination shell, associated with the next nearest neighbors, depended on the Zr concentration. For the catalyst with a higher Zr content, only one peak (2.8 Å) was observed. The catalyst with 0.3 wt % Zr/SMAO presented two small peaks at 2.8 and 3.8 Å. Polymers produced with the supported catalysts presented lower crystallinity and higher molar mass and polydispersity values in comparison to that produced by the homogeneous one. Gel permeation chromatogram deconvolution suggested the presence of four catalyst sites for the supported systems.
 J Appl Polym Sci 112: 563–571, 2009

Key words: computer modeling; metallocene catalysts; modeling; NMR; polyolefins

INTRODUCTION

A great part of the literature devoted to metallocene in polymerization catalysts has dealt with studies concerning the heterogenization of such catalyst systems. A solution polymerization process requires the separation of the polymer and the removal, recovery, and purification of the solvent. On the other hand, gas-phase processes have lower costs and energy consumption. As most of the existing polymerization plants run slurry- and gas-phase processes with heterogeneous systems, the homogeneous metallocenes must be heterogenized on a support if application to those processes is aimed. Moreover, the heterogenization of metallocene is necessary to prevent reactor fouling with finely dispersed polymer crystals, to prevent excessive swelling of polymers, and to produce polymer particles of a desired regular morphology.

In the last decade, many attempts have been made to heterogenize metallocene compounds. Different preparatory routes are described in the literature that have aimed to develop supported metallocene catalysts that could replace, without larger costs, heterogeneous Ziegler–Natta catalysts in industrial plants.[1] Silica is the most used carrier. Nevertheless, other supports have also been evaluated, such as Mobil Composition Matter-41 (MCM-41), Santa Barbara Amorphous 15 (SBA-15),[2] polymers,[3] and silica chemically modified with agents such as methyl aluminoxane (MAO) or perfluorophenylborate,[4] just to mention a few. Zirconocene systems synthesized *in situ*[5] or on hybrid silica[6,7] are also examples of the preparation of supported metallocene catalysts.

Another approach to the production of supported metallocene resides in the so-called *in situ* immobilization, in which the components (catalyst and support) are directly contacted in the reactor. Supported metallocenes, such as Ethylene bis(indenyl) zirconocene dichloride ($EtInd_2ZrCl_2$), prepared by the *in situ* immobilization technique have been evaluated for ethylene homopolymerization and copolymerization.[8–11] In previous studies, we examined propylene

Correspondence to: J. H. Z. dos Santos (jhzds@iq.ufrgs.br).
Contract grant sponsor: Conselho Nacional de Desenvolvimento Cientifico e Tecnológico (National Consel of Technological and Scientific Development) (CNPq)–Recursos Humanos em Áreas Estratégicas (Human Resources in Strategic Areas) (RHAE).

homopolymerization with *in situ* immobilized *rac*-dimethylsilylenebis(indenyl)zirconium dichloride [$Me_2Si(Ind)_2ZrCl_2$] as a catalyst and commercial methyl aluminoxane modified silica (SMAO) as a support. The effect of common alkylaluminum cocatalysts on catalyst activity in propylene polymerization and on polymer properties was evaluated.[12–14] The use of common alkylaluminums, such as triethylaluminum (TMA) or Triisobutyl aluminum (TIBA), reduces the possibility of leaching the catalyst from the surface, as reported for supported metallocenes.[15] Also, if one considers that the determination of the isotherm adsorption allows one to know the maximum surface loading regarding these complexes,[12] the use of a very low concentration, far from the saturation level, guarantees that there should be enough available sites on the surface for zirconocene grafting. Support morphology replication phenomena were also observed for polymers produced by these *in situ*-supported catalysts.[14]

In this study, we prepared supported $Me_2Si(Ind)_2ZrCl_2$ systems grafted on SMAO, bearing different Zr contents, which were evaluated in ethylene polymerization. Two systems were characterized by extended X-ray absorption fine structure (EXAFS) in the Zr edge. EXAFS is a very powerful tool that allows the determination of bond distance at the atomic level and the number of neighbors. The aim of this study was to correlate structure of such systems with the catalyst activity and polymer properties. The results are discussed according to a theoretical model based on the Ziegler group work and the application of a molecular mechanics, version 2 (MM2) calculation to a model of MAO–zirconocene interaction.

EXPERIMENTAL

Materials

All of the experiments were performed under an inert atmosphere with the Schlenk technique. The catalyst $Me_2Si(Ind)_2ZrCl_2$ (Witco, Cambridge, MA), SMAO (23 wt % Al/SiO_2, Witco), and isoprenylaluminum (IPRA; Akzo) were used without purification. Ethylene was used as received from the manufacturer (Copesul, Triunfo, Brazil) without any further purification. Toluene and hexane were purified by refluxing over sodium and by distillation. Hexane was degassed by bubbling nitrogen before each reaction.

Preparation of the supported catalysts

Several catalyst solutions bearing Zr concentrations corresponding to contents between 0.1 and 1.5 wt % Zr/SMAO were contacted with SMAO at room temperature for 30 min. The resulting slurry was washed with 15 × 2 mL of toluene and vacuum-dried, and the final metal content in the resulting solid was determined by Rutherford backscattering spectrometry (RBS).

Catalyst characterization

RBS

Zirconium loadings in catalysts were determined by RBS with He^+ beams of 2.0-MeV incident light on homogeneous tablets of compressed powder of the catalyst systems. The principle of RBS is to place a sample in the pathway of a monoenergetic ion beam coming from an ion accelerator and to detect the particles that are elastic scattered in the Coulombic field of the sample atomic nuclei. The most common incident beam is He^+, and the detector (normally, a surface barrier detector is used to detect the scattered particles) is usually placed at 165° with respect to the incidence direction of the beam, which characterizes a backscattering geometry. Each RBS spectrum can be decomposed in the Zr, Si, and O signals, which give rectangular-shaped individual contributions, which add up to the experimental spectrum. Among other factors, the energy of the scattered particles depends on the energy of incidence, the atomic masses of the atoms involved, and the depth in the sample where the scattering event occurred. The kinetic energy that is lost depends on the composition of the sample and on the length of the trajectory (or depth) of the incident ion in the material. On the other hand, the height of the signal corresponding to a certain element (number of counts) is proportional to the density of that element in the sample. The Zr/Si atomic ratio, for instance, can be determined from the ratio of the two signal heights (Zr/Si), and the metal loading is then calculated by converting atomic ratios (Zr/Si) into weight ratios (Zr/SiO_2). For an introduction to the method and applications of this technique, see ref. 16.

Nitrogen adsorption

A Micrometeritics Gemini instrument was used for the nitrogen sorption studies. The samples were preheated at 80°C for 12 h *in vacuo* before each measurement. The specific surface area was determined by the Brunauer–Emmett–Teller method at −196°C in the partial pressure range $0.01 < P/P_0 < 0.25$ (where P_0 is the vapor pressure of the adsorbate at the absorption temperature). The total pore volume was obtained from the N_2 desorption isotherm.

EXAFS

The X-ray absorption spectroscopy experiments were performed at the X-ray absorption spectroscopy (XAS) beam line[17] National Synchrotron Light Laboratory of

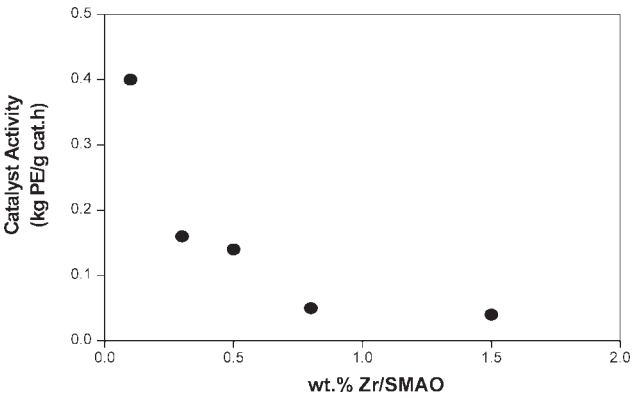

Figure 1 Catalyst activity of $Me_2Si(Ind)_2ZrCl_2$ supported on SMAO.

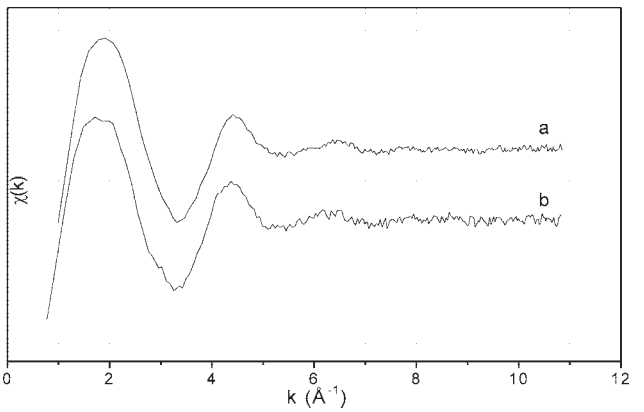

Figure 2 EXAFS spectra at the Zr–K edge: catalyst with (a) 0.8 and (b) 0.3 wt % Zr/SMAO (χ = crystallinity).

Brazil (Campinas, Brazil) with a Si(220) monochromator and vertical slits of 1.0 mm. Data were recorded at room temperature in transmission mode with two ion chambers filled with argon. Pellets of the catalysts powders were prepared in a glovebox and covered with Kapton tape to avoid air oxidation.

The EXAFS spectra were acquired in the range 17,870–18,440 eV with 2-eV steps and 4 s/pt. Several scans were collected for each catalyst; in the case of the one with lower Zr content, 10 scans were averaged to improve the signal-to-noise ratio.

The EXAFS spectra were analyzed by a standard procedure of data reduction, with the X-ray absorption spectroscopy data analysis under Microsoft Windows (WINXAS) code.[18] A linear function was used in the background subtraction, and a polynomial function was used to simulate the atomic absorption. A Fourier transform (FT) in the photoelectron vector (k) range 2.9–9 $Å^{-1}$ was performed with a Bessel window. Structural parameters were obtained from least squares fitting in r-space with theoretical phase shift and amplitude functions obtained from the FEFF code.[19]

In the fit were determined the coordination number (N), interatomic distance (R), Debye Waller factor (σ), and energy shift. For the coordination shell, the passive electron reduction factor was determined from $Me_2SiInd_2ZrCl_2$ for Zr—C bonds and kept fixed at 0.89 for the catalysts samples. For the next nearest neighbors, the passive electron reduction factor value was kept at 1. We performed the analysis by keeping the energy shifts fixed at −2.0 eV for the Zr—C pair and 3.7 eV for the Zr—Al pair. In the fitting procedure, the number of free parameters did not exceed the number of independent data points given by the Nyquist theorem.[20]

Polymerization

Polymerization reactions were performed in a 1.5-L stainless steel reactor equipped with a mechanical stirrer, a constant-temperature circulator, and inlets for argon and ethylene. The reactor was filled with the supported catalyst (Al/Zr = 500 mol/mol), 0.75 L of hexane, and IPRA. When the mixture reached 60°C, the reactor was pressurized with ethylene up to 6.0 bar (partial pressure) for 60 min. Homogeneous polymerizations were performed under the same conditions with MAO (Al/Zr = 500) as a cocatalyst instead of IPRA. Polymers were precipitated by acidified (HCl) ethanol and dried *in vacuo* at 90°C for 4 h.

Polymer characterization

The crystallinity (χ_c), melting temperature (T_m), and crystallization temperature were determined with a TA Instruments 2920 differential scanning calorimeter according to ASTM D 3417/97 and ASTM D 3418/97. Two scans were performed, but only the results of the second scan are reported. The heating rate was 10°C/min in the temperature range 30–220°C. Molar mass distributions were determined by high-temperature gel permeation chromatography (GPC) with a 150 C Waters instrument equipped with four GMHXL-HT columns (TosoHaas) at 138°C. 1,2,4-Trichlorobenzene was used as the

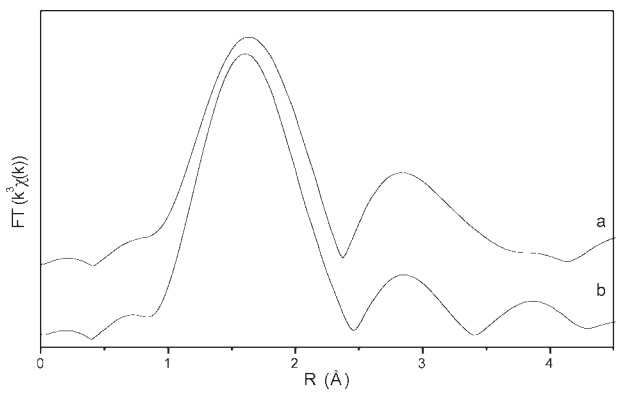

Figure 3 FTs of the EXAFS signal over the k range 2.9–9 $Å^{-1}$: catalyst with (a) 0.8 and (b) 0.3 wt % Zr/SMAO (χ = crystallinity).

TABLE I
Structural Parameters Obtained from the Fitting: *N*, *R*, and σ

Zr content (%)	Pair	*N*	*R* (Å)	σ^2 (Å^2)
0.8	Zr—C	5.6 ± 1.0	2.22 ± 0.02	0.0106 ± 0.0021
	Zr—Al	0.8 ± 1.0	3.40 ± 0.04	0.0043 ± 0.0009
0.3	Zr—C	5.1 ± 1.0	2.23 ± 0.02	0.0061 ± 0.0012
	Zr—Al	0.4 ± 1.0	3.43 ± 0.04	0.0081 ± 0.0014
	Zr—Al	0.4 ± 1.0	4.12 ± 0.04	0.0081 ± 0.0016

mobile phase. The columns were calibrated with 18 polystyrene and 3 polyethylene (PE) standards. The deconvolution of the polymer molar mass distribution was performed with an Excel spreadsheet. To obtain the best fit between the measured GPC curve and the fitted GPC curve (sum of the deconvoluted curves), Excel's Solver routine was used to minimize the sum of the squares of the differences between the measured and the fitted GPC curves ($\Sigma\Delta^2$). For each GPC curve, we carried out the deconvolution process considering 1, 2, 3, or 4 curves or peaks. In all of the results presented in this article, the parameter $\Sigma\Delta^2$ had the lowest possible value, without overlapping of the curves or peaks.

Theoretical studies with MM2

The software was provided by Cambridge Soft and the MM2 version was incorporated to Chem3D 5.0 (1999), which uses a modified version of an Allinger MM2 force field. The main incorporated functions to Allinger's MM2 force field are a charge–dipole interaction term, a quartic stretching term, cutoffs for electrostatic and Van der Waals terms with a 5° order polynomial switching function, automatic π system calculations, and torsion and nonbonded constraints. The parameters table of Chem3D contains many adjustable parameters that allow one to correct many of the potential functions in outlying situations.

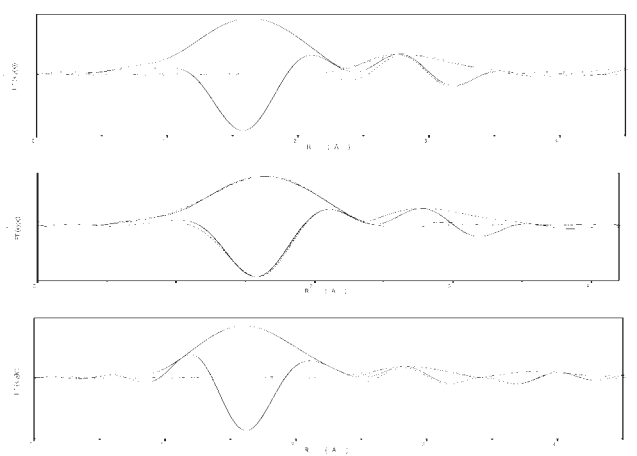

Figure 4 itting of the FT modulus and imaginary part; the experimental data are the solid lines, and the fittings are the dash–dot lines: fit of the (a) coordination shell with a Zr—C bond for the catalyst with 0.8 wt % Zr/SMAO content, (b) next nearest neighbor peak with a Zr—Al bond for the catalyst with 0.8 wt % Zr/SMAO content, and (c) next nearest neighbor peaks with two Zr—Al bonds for the catalyst with 0.3 wt % Zr/SMAO content (χ = crystallinity).

RESULTS AND DISCUSSION

Metal loading and catalyst activity

The maximum surface loading for a certain catalyst can be obtained by the determination of its adsorption isotherm. In a previous study, $Me_2Si(Ind)_2ZrCl_2$ solutions containing between 0.5 and 5.0 wt % Zr/SMAO were put in contact with commercial SMAO.[12] The saturation level was reached at about 2.0 wt % Zr/SMAO. Almost all metallocene present in the toluene solution seemed to have been immobilized on the SMAO surface for contents below 2.0 wt % Zr/SMAO. Such behavior suggested strong interactions between the catalyst and the surface.

The effect of variation of Zr content immobilized on SMAO lower than the saturation level was evaluated on ethylene polymerization (Fig. 1). The highest catalyst activity was observed for 0.1 wt % Zr/SMAO. As the grafted content increased, catalyst activity decreased up to 0.8 wt % Zr/SMAO and remained roughly constant for 1.5 wt % Zr/SMAO. The decrease in catalyst activity with increasing catalyst content was already reported in the literature, and it was attributed to the possibility of bimolecular deactivation reactions due to greater proximity among catalyst centers in high Zr contents.[21] Under the same experimental conditions, homogeneous

TABLE II
Polymer Characteristics for the Different Catalyst Systems

Zr/SMAO (wt %)	T_m (°C)	χ_c (%)	M_n (kg/mol)	M_w/M_n
$Me_2Si(Ind)_2ZrCl_2$	133	59	67	2.5
0.1	132	36	71	4.0
0.3	132	37	59	6.9
0.5[a]	129	43	69	5.6
0.8	132	41	63	5.9
1.5	132	44	79	4.0

[a] The polymer did not completely dissolve.

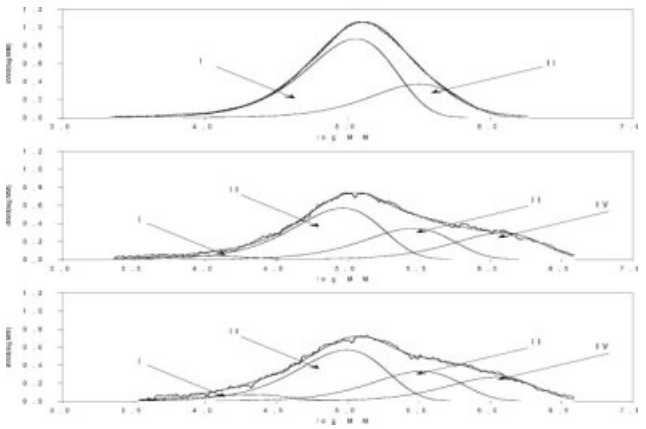

Figure 5 Molar mass distribution deconvolution of the polymers by the (a) homogeneous system, (b) supported system bearing 0.3 wt % Zr/SMAO, and (c) supported system bearing 0.8 wt % Zr/SMAO.

$Me_2Si(Ind)_2ZrCl_2$ in the presence of MAO as a cocatalyst (Al/Zr = 500) produced 5.1 kg of PE (g of catalyst)$^{-1}$ h^{-1}. Homogeneous catalysts usually have higher catalyst activity than supported ones because, in the former, all molecules are potentially active. Specifically, in the case of immobilized metallocene catalysts, depending on the Brönsted acidity and the OH group density, some inactive species, such as μ-oxo covalently bonded species or bidentated ones, can be formed. It is believed that about 1% of the grafted species are indeed active.[22] Also, the silica surface itself plays the role of a huge ligand in the supported catalysts, and this steric hindrance renders difficult accessibility to the catalyst sites. Attempts to map Zr distribution on the catalyst grain by a scanning electron microscope coupled to an energy-dispersive X-ray detector were not successful, probably because of the low metal concentration.

The rate of polymerization is often diffused-limited. Zirconocene sites near a pore mouth or on the surface would contribute more to the observed rate than the sites inside the pores. Therefore, the reactivity of these catalysts would be higher in the case of lower loading samples because most of the catalyst species should be grafted on the uttermost surface. The support surface areas measured by nitrogen adsorption and calculated by the Brunauer–Emmett–Teller model were 185, 160, and 145 m^2/g, respectively for SMAO and the supported catalysts bearing 0.3 and 0.8 wt % Zr/SMAO. Indeed, the surface area showed a reduction of about 22% when we compared the surface area from the support and that of the resulting catalyst with 0.8 wt % Zr/SMAO. Nevertheless, a reduction of about 85% in catalyst activity was observed when we compared these two catalysts (see Fig. 1). Therefore, although diffusion might have been influenced as the grafted metal content increased, it could not thoroughly justify the reduction in catalyst activity. These two catalysts were further analyzed by EXAFS.

EXAFS allows one to get information on the environment around the Zr center by measuring the X-ray absorption in the Zr–K edge. EXAFS has already been used for the characterization of metallocenes.[23–25] In a previous study, EXAFS analysis in the Zr edge showed that, for hybrid-supported metallocene catalysts, systems bearing Cp_2ZrCl_2 and Bis-n-butyl cyclopentadienyl zirconocene dichloride [$(nBuCp)_2ZrCl_2$] in a 1 : 3 molar ratio afforded more disordered systems.[26]

The Zr–K edge EXAFS spectra of the $Me_2Si(Ind)_2ZrCl_2/MAO/SiO_2$ catalysts with Zr contents of 0.8 and 0.3 wt % Zr/SMAO were quite similar (Fig. 2). The shape of the signal was a damped sine function that mostly came from the coordination shell. The beat pattern shoulder observed at about 6 Å^{-1} indicated the contribution of the next nearest neighbors to the EXAFS signal.

The FTs (Fig. 3) of both samples displayed one main peak at about 1.5 Å related to the coordination shell. The number and the intensity of the peaks beyond the coordination shell associated with the next nearest neighbors depended on the Zr concentration. For the catalyst with a higher Zr content, only one other peak at about 2.8 Å was observed. The catalyst with 0.3 wt % Zr/SMAO had two small peaks at 2.8 and 3.8 Å. The FTs were also performed with a different apodization window and *k* extension; the number and shape of the peaks in the FTs were identical, which means that the one at 3.8 Å corresponded to an *R* and was not an artifact of the data handling.

The quantitative analysis yielded the parameters presented in Table I. The refinement of the coordination shell was performed with different possibilities of scattering atoms, such as carbon and/or chlorine atoms, considered. The best fits were obtained for both samples with a single carbon shell considered as first neighbor atoms, and an excellent fit quality was obtained in both cases. The values for Zr—C and Zr—Al bond distance were close to those

TABLE III
M_n Values and Percentages of the Peaks Resulting from the Deconvolution of the GPC Chromatograms

	Peak I/site I		Peak II/site II		Peak III/site III		Peak IV/site IV	
Zr/SMAO (wt %)	M_n (kg/mol)	%	M_n (kg/mol)	%	M_n (kg/mol)	%	M_n (kg/mol)	%
0.3	5.5	3	46	45	144	28	605	24
0.8	10	6	49	45	164	27	551	22

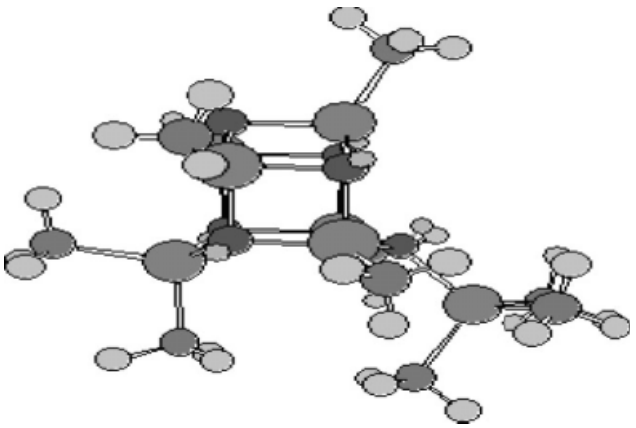

Figure 6 MAO cage model according to ref. 33.

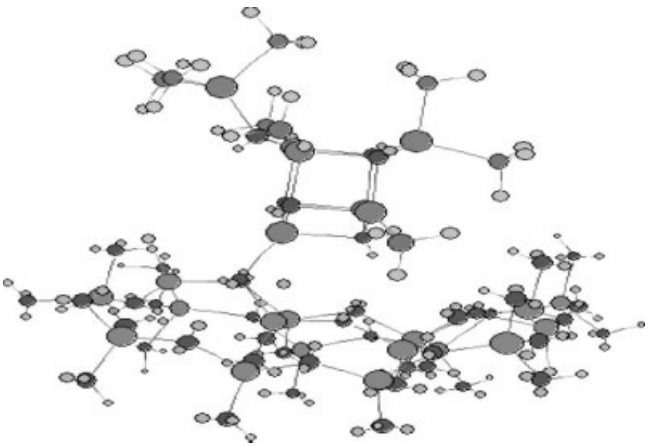

Figure 7 MAO cage model reacted with the SiO_2 surface.

reported in the literature.[23] Figure 4(a) shows the fit obtained for the catalyst with a higher Zr content.

In the analysis of the next nearest neighbors, different atoms were considered. Among the possibilities, silicon, aluminum, chlorine, and oxygen atoms were examined. Because of the similarity of phase shift and amplitudes[27] of aluminum and silicon atoms, it is practically impossible to distinguish them in an EXAFS fit. The best fit results were obtained for the catalyst with 0.8 wt % Zr/SMAO with a single Al or Si shell considered [Fig. 4(b)]. Nevertheless, with the saturation level of MAO on silica considered to be about 8–10 wt % Al/SiO_2[28] and with the fact that commercial SMAO has about 23 wt % Al/SiO_2, it was very likely that the next nearest neighbor atoms were aluminum ones.

In the case of the catalyst with 0.3 wt % Zr/SMAO, the two peaks beyond the coordination shell were fitted with two Zr—Al shells considered, and a good fit quality was obtained [Fig. 4(c)].

According to Table I, the number of neighbors (C and Al) was roughly the same. The number of C(5) may have resulted from the constructive and destructive interference of the signal, which was a mean. In the case of 0.3 wt % Zr/SiO_2, two Al shells were detected: one at 3.43 Å and another at 4.12 Å, with the latter absent in the case of the 0.8 wt % Zr/SiO_2 system. The longer Zr—Al distance may have guaranteed a weaker zirconocenium ion pair ($[SiO—Al(Me)O^-]$ $[R_2ZrMe]^+$ originating from the reaction between the zirconocene and the SMAO surface and stabilized by the multicoordinative crown aluminoxane species. This weaker interaction rendered the system more prone to dissociation during the olefin coordination and allowed the propagation reaction to grow further, which in turn afforded a higher catalyst activity.

Polymer characteristics

The obtained PEs were characterized by GPC and differential scanning calorimetry (Table II). The detected T_m at 132°C was typical of high-density PE. χ_c was lower for PEs obtained with supported catalysts and increased as Zr content increased. The polymers obtained with heterogeneous catalysts presented molar masses higher than those obtained with the homogeneous one. This behavior was already observed and attributed to the blocking of one of the sides of the polymerization active sites by the support, which hindered the deactivation step. In other words, β-elimination transfer between two metallocene centers was hindered, which resulted in a larger growth of the polymer chain and, therefore, in a higher molar mass.[29] The polydispersity [weight-average molecular weight (M_w)/number-average molecular weight (M_n)] was between 4.0 and 6.9; that is, the single-site nature of the metallocene seemed not to be retained after grafting. The intrinsic heterogeneity from the support surface might have afforded different potential catalyst sites.

The molar mass distribution of polymers can be described by Flory's most probable distribution, and mathematical models can be useful tools in gaining a

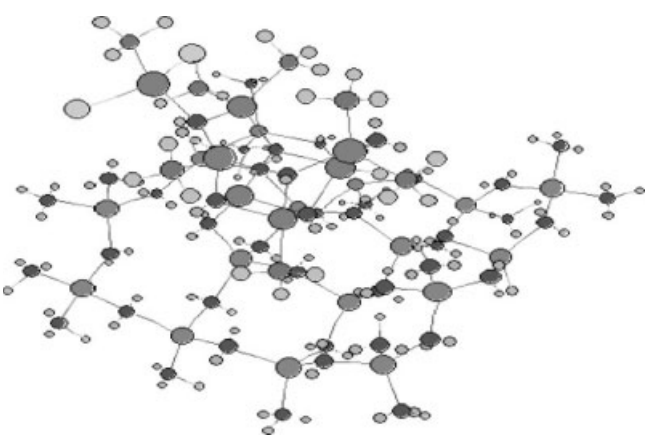

Figure 8 Counterion with two Cl atoms and one Al atom from the supported MAO cage model (steric energy = −557.4 kcal/mol).

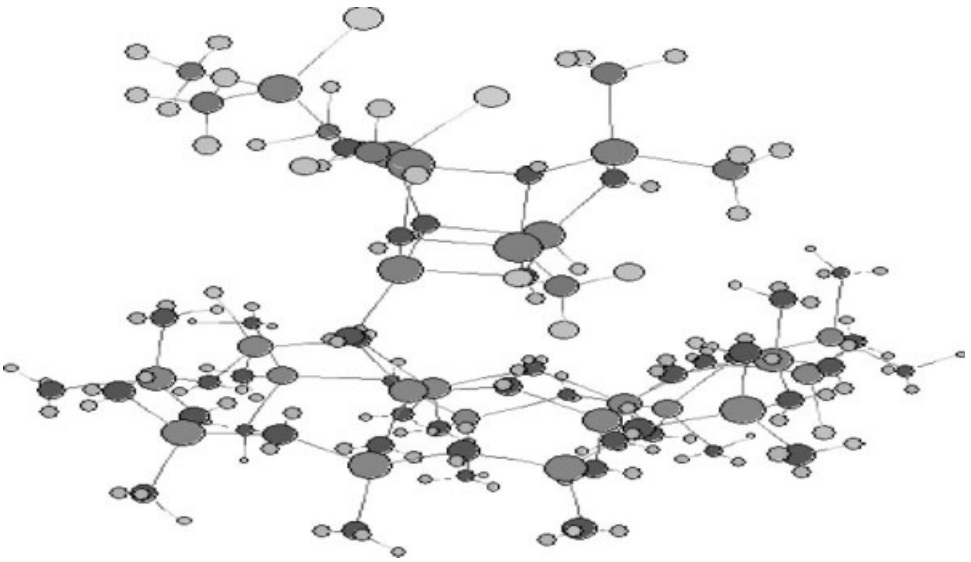

Figure 9 Counterion with two Cl atoms included in the supported MAO cage model (steric energy = −558.4 kcal/mol).

better understanding of a process or a system.[30–32] Figure 5 shows the GPC curves for the polymers obtained with the homogeneous and supported catalysts. The best deconvolution curves of the supported catalysts suggested the presence of four polymeric species, which presented different molar masses (Table III). Such results suggest the presence of more than one catalyst site on the support surface. PEs with a broad polydispersity show greater flowability in the molten state at high shear rate, which is important for blowing and extrusion techniques. Many efforts have been made to produce polymers by metallocene catalysts with a broader polydispersity.[1]

A theoretical model was constructed to explain the results observed in terms of catalyst activity and data from EXAFS analysis.

Theoretical model

The MAO model we used was similar to that proposed by Zurek and Ziegler:[32] a cage with coordinated TMA in which all O atoms are tricoordinated to three Al atoms, and the cage includes two $AlMe_2$ groups. One $AlMe_3$ molecule is coordinated to the cage (Fig. 6).

Figure 7 shows the MAO model reacted with the silica surface, with tetrahedral Si considered, and the formation of an Al—O—Si bond, with the loss of an H (from the surface) and a methyl group (from the MAO model).

According to the Zurek–Ziegler model, the interaction of the zirconocene with MAO produces a compound with two Cl atoms on the same Al (from the cage) or in two different Al atoms (also from the cage) and a zirconocene with a Zr^+—Me bond. Interaction of the zirconocene with MAO is considered to take place through chlorine (from $OAlMe_2Cl$) or through O_2AlMe_2. The interaction of one or two zirconocenes with the same MAO cage (supported) is also taken into account. Then, the zirconocene interacts with the MAO model in sequence, according to the following reactions:

$$Al—Me + ZrCl_2 \rightarrow Al—Cl + ZrClMe \quad (1)$$

$$ZrClMe + Al—Me— \rightarrow Zr^+—Me + AlCl^-—Me \quad (2)$$

Two possibilities were then explored: different Al atoms for reactions (1) and (2) or similar Al [and, therefore, in reaction (2), the second chlorine is transferred to Al—Cl instead of Al—Me]. The preferred conformation has two Cl atoms in two different Al atoms. Figures 8 and 9 show the two different resulting structures in the MAO model.

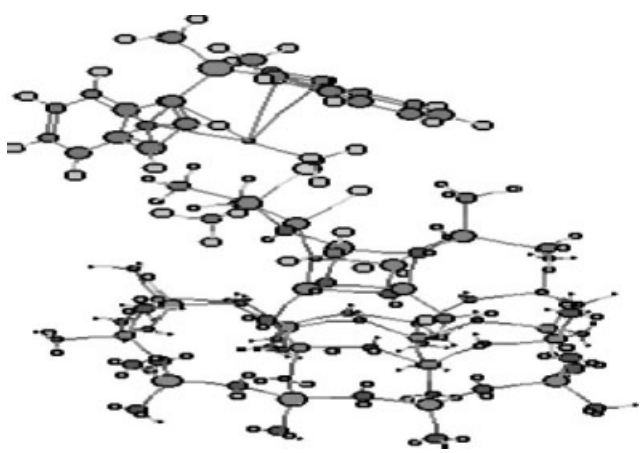

Figure 10 Zircocation coordinated through $OAlMe_2Cl$ conformation 1 (steric energy = −579.8 kcal/mol).

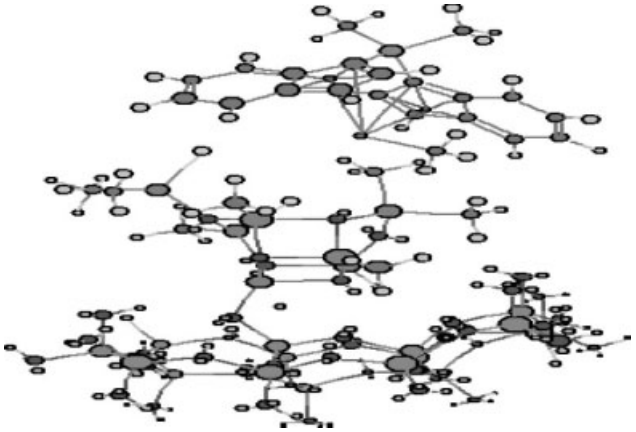

Figure 11 Zircocation coordinated through $OAlMe_2Cl$ conformation 1 (steric energy = −556.2 kcal/mol).

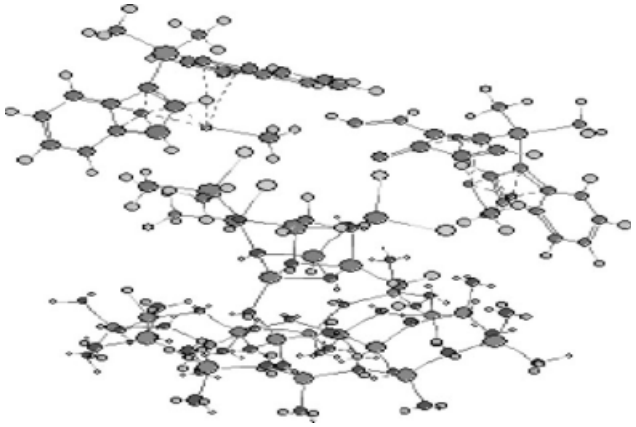

Figure 12 Two active sites on a supported MAO cage model.

The zirconocene can be coordinated through chlorine (conformation 1) or through oxygen (conformation 2), as shown in Figures 10 and 11. When coordinated through O, the zirconocene site is considered to be a dormant site.[33]

Table IV shows the structural parameters for each of the conformations. In addition, a situation in which two zirconocenes are considered to be reacted with one cage is also included. This situation is considered to take place with 0.8 wt % Zr/SMAO.

Comparing the EXAFS (Table I) and MM2 data (Table IV), one can see that there was a very good agreement for Zr—Al distance. In the case of 0.3 wt % Zr/SMAO, there was a distribution of active and dormant sites, bearing different Zr—Al (and Zr—O) bond distances. For the 0.8 wt % Zr/SMAO supported system, with a higher concentration of zirconocene, the remaining available sites for activation on the supported MAO cage could have reacted with a second zirconocene. Repulsion between the zirconocenes made the Al—Zr distances shorter. In this case, the model must accommodate two negative charges, and therefore, the distances were shorter because two positive charges were involved. Also, steric crowding was higher, and then, propagation constants were probably lower (Fig. 12). The coordination of Zr was high when we considered the methyl group, the two Cp centroids, the Al, and the bridge chlorine or methyl with the Al. In sum, for higher Zr contents, no dormant sites would have been present, but the steric hindrance increased because of the interaction of different zirconocenes on the MAO cage surface, and the resulting tight ion pairs bore shorter Al—Zr bond distances. This would explain the lower observed catalyst activity on ethylene polymerization.

TABLE IV
Structural Parameters Obtained with the MM2 Calculations

	Zr—Al (Å)	Zr—O (Å)	Zr coordination
Conformation 1	3.764	5.45	6/7
Conformation 2	4.080	4.041	5/6
Two zirconocenes	3.559/3.50	5.259/4.06	6/7 + 5/6

CONCLUSIONS

The catalyst activity of supported systems resulting from the grafting of $Me_2Si(Ind)_2ZrCl_2$ on SMAO seemed to be dependent on the Al/Zr ratio and decreased as the Zr content increased. The neighborhood of the resulting grafted species, according to EXAFS measurements, seemed to vary with the Zr content: two Zr—Al moieties were found to be present in the case of 0.3 wt % Zr/SMAO, but only one was present for 0.8 wt % Zr/SMAO.

Surface heterogeneity was also reflected in the polymer properties, especially in the polymer polydispersity, which was higher than that observed with the homogeneous catalyst.

Theoretical calculation could model the interaction for low and higher metal contents: the steric effect among catalyst zirconocene species on the MAO–silica surface accounted for the observed decrease in catalyst activity.

This research was partially performed at the National Synchrotron Light Laboratory of Brazil (project XAS 951/01).

References

1. Severn, J. R.; Chadwick, J. C.; Duchateau, R.; Friederichs, N. Chem Rev 2005, 105, 4073.
2. Doug, X.; Wang, L.; Jiang, G.; Zhao, Z.; Sun, T.; Yu, H.; Wang, W. J Mol Catal A 2005, 240, 239.
3. Wu, L.; Zhou, J.-M.; Lynch, D. T.; Wanke, S. E. Appl Catal A 2005, 293, 180.
4. Panchenko, V. N.; Danilova, I. G.; Zakharov, V. A.; Paukshtis, E. A. J Mol Catal A 2005, 225, 271.

5. Bortolussi, F.; Broyer, J.-P.; Spitz, R.; Boisson, C. Macromol Chem Phys 2002, 203, 2501.
6. dos Santos, J. H. Z.; Ban, H. T.; Teranishi, T.; Uozumi, T.; Sano, T.; Soga, K. J Mol Catal A 2000, 158, 541.
7. Guo, Y.; Zhang, X.; Dong, W. J Mol Catal A 2005, 237, 45.
8. Chu, K. J.; Soares, J. B. P.; Penlidis, A. J Polym Sci Part A: Polym Chem 2000, 38, 462.
9. Chu, K. J.; Soares, J. B. P.; Penlidis, A. J Polym Sci Part A: Polym Chem 2000, 38, 1803.
10. Lee, H. W.; Ahn, S. H.; Park, Y. H. J Mol Catal 2003, 194, 19.
11. Jongsomjit, B.; Praserthdam, P.; Kaewkrajang, P. Mater Chem Phys 2004, 86, 243.
12. Franceschini, F. C.; Tavares, T. T. R.; Greco, P. P.; Bianchini, D.; Stedile, F. C.; Galland, G. B.; dos Santos, J. H. Z.; Soares, J. B. P. J Mol Catal A 2003, 202, 127.
13. Franceschini, F. C.; Tavares, T. T. R.; Greco, P. P.; Galland, G. B.; dos Santos, J. H. Z.; Soares, J. B. P. J Appl Polym Sci 2005, 95, 1050.
14. Franceschini, F. C.; Tavares, T. T. da R.; dos Santos, J. H. Z.; Soares, J. B. P. Macromol Chem Phys 2004, 205, 1525.
15. McKittrick, M. W.; Jones, C. W. J Catal 2004, 227, 186.
16. Stedile, F. C.; dos Santos, J. H. Z. Phys Status Solidi A 1999, 173, 123.
17. Tolentino, H. C. N.; Ramos, AY.; Alves, M. C. M.; Barrea, R. A.; Tamura, E.; Cezar, J. C.; Watanabe, N. J. Synchrotron Rad 2001, 8, 1040.
18. Ressler, T. J Phys 1997, 4, 269.
19. Zabinsky, S. I.; Rehr, J. J.; Ankudinov, A.; Albers, R. C.; Eller, M. J Phys Rev B 1995, 52, 2995.
20. Lytle, F. W.; Sayers, D. E.; Stern, E. A. Phys B 1989, 158, 701.
21. Bianchini, D.; Stedile, F. C.; dos Santos, J. H. Z. Appl Catal 2004, 261, 57.
22. Muñoz-Escalona, A.; Méndez, L.; Sancho, J.; Lafuente, P.; Peña, B.; Michels, W.; Hidalgo, G.; Martinez-Nuñez, M. F. In Metalorganic Catalysts for Synthesis and Polymerization; Kaminsky, W., Ed.; Springer: Heidelberg, 1999; p 381.
23. Jezequel, M.; Dufaud, V.; Ruiz-Garcia, M. J.; Carrillo-Hermosilla, F.; Neugebauer, U.; Niccolai, G. P.; Lefebvre, F.; Bayard, F.; Corker, J.; Fiddy, S.; Evans, J.; Broyer, J.-P.; Malinge, J.; Basset, J.-M. J Am Chem Soc 2001, 123, 3520.
24. Mäkela-Vaarne, N. I.; Nicholson, D. G.; Ramstad, A. L. J Mol Catal A 2003, 200, 232.
25. O'Brien, S.; Tudor, J.; Maschmeyer, T.; O'Hare, D. Chem Commun 1997, 1905.
26. Loureiro, S. R.; Silveira, F.; Pires, G. P.; Alves, M. C. M.; Stedile, F. C.; dos Santos, J. H. Z.; Bichinho, K. M.; Teranishi, T. X-Ray Spec 2005, 34, 101.
27. Koningsberger, D. C.; Prins, R. X-Ray Absorption: Principles, Applications and Techniques of EXAFS, SEXAFS and XANES in Chemical Analysis; Wiley: New York, 1988; Vol.92.
28. dos Santos, J. H. Z.; Dorneles, S.; Stedile, F. C.; Dupont, J.; Forte, F. C.; Baumvol, I. J. R. Macromol Chem Phys 1997, 198, 3529.
29. Kaminsky, W.; Renner, F. Makromol Chem Rapid Commun 1993, 14, 239.
30. Kissin, Y. V. Makromol Chem Macromol Symp 1993, 66, 83.
31. Kissin, Y. V. J Polym Sci Part A: Polym Chem 1995, 33, 227.
32. Dubé, M. A.; Soares, J. B. P.; Penlidis, A.; Hamielec, A. E. Ind Eng Chem Res 1997, 36, 966.
33. Zurek, E.; Ziegler, T. Prog Polym Sci 2004, 29, 107.